

Impact of long-range desert dust transport on coastal East Asia: analysis of urban dust concentration and wet deposition with model simulation

Zhenxi Zhang^{1,2} · Wen Zhou³ · Mark Wenig⁴ · Liangui Yang¹

Received: 28 June 2016 / Accepted: 19 September 2016 / Published online: 21 October 2016
© Springer Science+Business Media Dordrecht 2016

Abstract Global Ozone Chemistry Aerosol Radiation and Transport (GOCART) model simulations for dust in 2007 are applied in this study to investigate the impact of long-range desert dust transport on the dust concentration and wet deposition in coastal cities of East Asia: Shanghai and Hong Kong. The temporal variation of dust concentrations in both Shanghai and Hong Kong exhibits a maximum in spring (May), with a majority of Gobi dust, which accounts for 88 % in Shanghai and 58 % in Hong Kong in the lower troposphere. Correspondingly, the peaks of convective and large-scale wet deposition in May in Shanghai are controlled by Gobi dust, with a contribution of 74–83 %. The wet deposition of dust in summer is affected mainly by strong convective precipitation and dominated by Taklamakan dust, with a contribution of 31–47 % in Shanghai and 19–37 % in Hong Kong, followed by Arabian and Karakum–Kavir dusts. The wet deposition in spring (April) is caused mainly by large-scale precipitation, with a majority of Gobi dust, which accounts for 57 % in Shanghai and 71 % in Hong Kong, followed by Sahara and Taklamakan dusts. The temporal variation of wet deposition of dust in Shanghai is affected mainly by the dust concentration, while the variation in Hong Kong is

controlled by both dust concentration and convective precipitation.

Keywords Dust · Wet deposition · Transport · Model simulation

Introduction

Dust particles, as a major aerosol component, are important in meteorological changes and biogeochemical cycles (Mahowald et al. 2005; McTainsh and Strong 2007; Shao et al. 2011). Mineral dust particles affect meteorological and climatic changes by absorbing and scattering the radiation in the atmosphere, as well as modifying the optical properties of clouds (Tegen 2003). All these effects relate to the loading of airborne dust particles and their vertical distribution in the atmosphere. Atmospheric mineral dust deposits in the ocean and on land to affect ecosystems by contributing to the transport of nutrient elements, i.e., phosphorus (P), iron (Fe), and nitrogen (N) (Nishikawa et al. 1991; Duce 1995; Prospero 1996; Okin et al. 2004; Jickells et al. 2005). But the content of nutrient elements, Fe for example, in the dust particles from different deserts is different, and this will lead to different effects on biogeochemical processes. To evaluate these meteorological and biogeochemical effects on regional and global scales, temporal and spatial variation of dust concentration and deposition, as well as the composition from different desert sources, must be assessed.

Coastal East Asia is one of the most intensively populated regions in the world, so the meteorological and biogeochemical effects of mineral dust particles over this region have important effects on human activities, especially in the large cities. In addition, long-range transport of desert dust on a global scale is steadily occurring, producing long-term

✉ Liangui Yang
yyb3006@sina.com

¹ Research Institute of Fluid Dynamics, School of Mathematic Science, Inner Mongolia University, Hohhot, China

² Department of Environmental Engineering, Inner Mongolia University of Technology, Hohhot, China

³ School of Energy and Environment, City University of Hong Kong, Hong Kong, Tat Chee Avenue, Kowloon, Hong Kong, China

⁴ Meteorologisches Institut, Ludwig-Maximilians-Universität, Munich, Germany

impacts on local climates and ecosystems in coastal East Asia. Because precipitation in coastal East Asia is often active and occurs far away from deserts, the wet deposition of dust that accompanies precipitation plays an important role in dust deposition in coastal East Asia. To study the temporal and spatial variations of dust concentration and wet deposition in coastal cities of East Asia, many kinds of observations can be implemented, for example, in situ observations and satellite observations (Kim et al. 2016), but observation data generally cannot differentiate between local dust contamination and long-range desert dust transport, and such data cannot be used to evaluate the composition from different desert sources. In this study, the atmospheric chemical transport model Global Ozone Chemistry Aerosol Radiation and Transport (GOCART) is implemented to separately simulate the transport of dust particles originating from deserts in Asia and Africa in order to quantitatively assess the contribution of dust from different desert sources to the dust concentration and wet deposition in coastal cities of East Asia.

The objective of this study is to investigate the temporal and spatial variations of the dust concentration and wet deposition in coastal cities of East Asia, as well as the composition from different desert sources to reveal the relationship between the contribution of desert dust and its transport and precipitation. The description and validation of the GOCART model are given in the “Model description” and “Validation of dust sources with satellite observations” sections. Analysis of the model results, including the characteristics of desert dust transport, concentration, and wet deposition, is presented in the “Dust transport to coastal East Asia,” “Variability and composition of urban dust concentration in coastal East Asia,” and “Variability and composition of urban wet deposition of dust in coastal East Asia” sections, respectively, followed by conclusions in the “Summary and Conclusions” section.

Model description

The Georgia Tech/Goddard GOCART 4.0 model is a chemistry transport model that simulates the major aerosol components in the atmosphere, including sulfate, mineral dust, black carbon, organic carbon, and sea salt, through the parameterization and calculation of the aerosol processes of emission, chemistry, advection, convection, diffusion, dry deposition, and wet deposition. The assimilated meteorological fields from the Goddard Earth Observing System Data Assimilation System (GEOS DAS) version 4 are applied to drive the GOCART model. The horizontal resolution of the GOCART model is 2° latitude by 2.5° longitude, and its vertical resolution is 30 layers from the ground to 0.01 hPa. Detailed information on the GOCART model can be found in previous publications (Allen et al. 1996; Chin et al. 2000,

2001, 2002, 2007; Ginoux et al. 2001; Zhang et al. 2014). Here we give a brief introduction of the major model components for dust simulation.

Emission of dust source

The GOCART model is restricted to dust particles with a radius of 0.1–10 μm, while the size distribution is modeled into five size bins. Ginoux et al. (2001) applied the empirical formulation by Gillette and Passi (1988) for dust uplifting as the algorithm of the dust emission scheme in GOCART, in which the flux F_p (unit: μg m⁻² s⁻¹) of size bin p is calculated by the expression:

$$F_p = C \cdot S \cdot s_p u^2 (u - u_t) \quad \text{if } u > u_t \quad (1)$$

where C , with the value of 1 μg s² m⁻⁵, is a dimensional factor; s_p is the fraction of size bin p within the soil; and u is the horizontal wind speed at the surface. S (unitless) is the dust source function and is represented by the fraction of alluvium available for wind erosion (Ginoux et al. 2001). S is calculated by the following expression:

$$S = \left(\frac{z_{\max} - z_i}{z_{\max} - z_{\min}} \right)^5 \quad (2)$$

where S is the probability of the sediments being collected in grid cell i with altitude z_i , and z_{\max} and z_{\min} mean the maximum and minimum altitudes in the surrounding 10° latitude by 10° longitude region, respectively. The parameter u_t is the threshold velocity for soil erosion, as determined by surface wetness and particle size:

$$u_t = 6.5 \sqrt{\frac{\rho_p - \rho_a}{\rho_a}} g \Phi_p (1.2 + 0.2 \log_{10} \omega) \quad \text{if } \omega < 0.5 \quad (3)$$

where ρ_a and ρ_p represent the air and particle densities, respectively; Φ_p is the particle diameter; and ω is the surface wetness, with the value being in the range from 0.001 to 1.

Aerosol optical depth

Aerosol optical depth (AOD), which reflects the attenuation of sunlight by a column of aerosol, can serve as a measure of aerosol column concentration. Given the aerosol type, mass, and wavelength, the AOD τ can be calculated by the formulation listed below:

$$\tau = B \cdot M_d \quad (4)$$

where M_d is the aerosol dry mass excluding the mass of water taken by the aerosol, and B is called the specific or mass extinction coefficient (m² g⁻¹), including all the humidification effects. Correspondingly, the value of B is related to the relative humidity (RH) and wavelength (Chin et al. 2002) and

is calculated from the optical property database in the Global Aerosol Data Set under the Mie-scattering theory (Koepke et al. 1997).

Wet deposition

Wet deposition of aerosols in the GOCART model includes the removal processes of large-scale precipitation and convective precipitation. The calculation method for dust is the same as that used for sulfate (Ginoux et al. 2001). The aerosols scavenged by convective precipitation are computed according to the convective mass transport operator. When an air mass is pumped in wet convective updrafts, a fraction of its aerosols will deposit. This fraction is called the scavenging efficiency, equal to 50 % in shallow wet convection (extending up to 2600 m altitude) and 100 % in deep wet convection. The aerosols scavenged by large-scale precipitation are computed using a first-order loss operator, which is parameterized using the method of Giorgi and Chameides (1986).

Separation of dust sources for the individual desert dust simulation

More than 90 % of the dust particles in the Earth's atmosphere are emitted from the deserts in Africa and Asia between 15° and 35° N (Chin et al. 2007), including six deserts: the Sahara Desert in Africa, the Taklamakan and Gobi deserts in China and Mongolia, the Arabian Desert in the Middle East, the Karakum and Kavir Deserts in Central Asia, and the Thar Desert in the Indian subcontinent.

In this study, the dusts emitted from these six deserts are simulated respectively. To simulate a desert dust individually, it is necessary to separate the dust source from other sources. First, the source region of the above six deserts is partitioned by setting a panel which covers the desert source (Fig. 1). Then in the simulation for an individual desert dust, the dust emission in the corresponding panel is retained while other desert dust emissions are ignored by setting the value of their emission flux as zero.

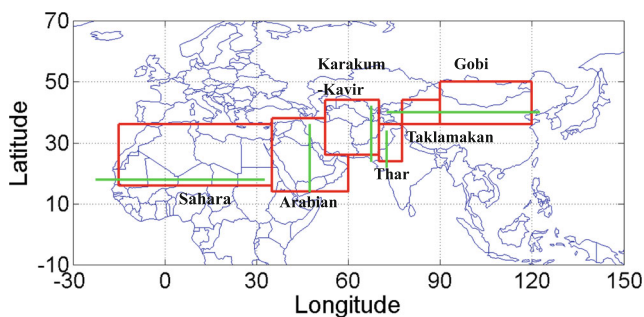


Fig. 1 Location of desert source regions (in the red panel) used in GOCART simulation cases, while the green line is the cross section used to show the vertical distribution of dust extinction

2007 is the latest year that can be simulated by GOCART 4.0. On the other hand, previous studies (Lee et al. 2010; Zhang et al. 2014) have found that the impact of long-range desert dust transport on coastal East Asia is largest in spring, with its majority coming from Gobi Desert. In this study, the dust emission of Gobi Desert in spring is represented with the UV Aerosol Index data from the Ozone Monitoring Instrument (OMI) satellite observations, and the interannual variability of the spring UVAI over the Gobi Desert during the period from 2005 to 2013 is presented in Fig. 2. It can be seen that the value of OMI UVAI over Gobi Desert region is 1.05 in 2007, which is 96 % of the temporal average value from 2005 to 2013 (1.10). Therefore, the Gobi dust emission in 2007 can be referring as the representative of its climatic mean value. Consequently, 2007 is selected as the simulation period in this study.

Validation of dust sources with satellite observations

The accurate calculation of dust emission flux plays an important role in the dust simulation because dust source is critical to the overall distributions of dust mass in the atmosphere and its deposition to the ground. Therefore, the dust sources simulated by GOCART are validated with the satellite observations. Firstly, the simulation for global dust sources is validated with the UVAI data from OMI. Then the simulations for individual desert dust source are validated with the dust extinction data at the wavelength of 532 nm from the Cloud-Aerosol Lidar and Infrared Pathfinder Satellite Observations (CALIPSO).

To validate the GOCART model simulation for global dust in 2007, the GOCART-simulated dust AOD at a wavelength of 550 nm is compared with the satellite-observed aerosol data. Because the satellite-observed AOD actually reflects not just desert dust but also other aerosol components, even reflecting mainly anthropogenic aerosols over regions with high population, the properties of dust distribution cannot be presented accurately by the satellite-observed AOD. Therefore, the UVAI data from the OMI is used in this study

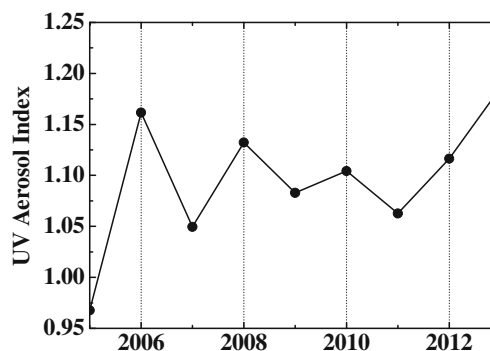


Fig. 2 The interannual variability of the spring UV Aerosol Index over Gobi Desert region (see Fig. 1) from 2005 to 2013

to present the properties of dust distribution and compare them with the simulated dust AOD. A positive value of UVAI comes mainly from desert dust because absorption by dust increases strongly toward the UV (Torres et al. 2007).

Figure 3 shows the distributions of UVAI from OMI and the comparisons with GOCART-simulated dust AOD at a wavelength of 550 nm for March–April–May (MAM) 2007, June–July–August (JJA) 2007, September–October–November (SON) 2007, and December–January–February (DJF) 2007. The model and satellite data give generally consistent spatial patterns of dust distribution and its seasonal variations, with the most prominent features of dust plumes over the major continental source regions being readily identified. But the calculated dust AOD cannot quantitatively represent the distribution of dust plumes, and several differences between UVAI and GOCART AOD are evident over the major dust source regions. The GOCART model substantially overestimates the dust AOD over the Taklamakan Desert in spring (MAM), summer (JJA), and autumn (SON). Over the Arabian Desert, on the other hand, GOCART underestimates the dust AOD in spring and summer. The dust AOD over the Sahara Desert is overestimated in autumn and underestimated in summer and winter (DJF).

The difference between the model simulation and satellite observations is actually related to the uncertainties involved in deriving the AOD from the model, of which we will discuss a few here. According to Eq. (4), the AOD at any given wavelength is determined by two quantities: the dry aerosol mass M_d and the mass extinction efficiency B . The aerosol dry mass M_d is determined by the emissions, transport, and deposition processes. Each of these processes is complex and highly uncertain. The accurate calculation of aerosol emission flux plays a significant role in determining the amount and distribution of aerosol mass in the atmosphere. The M_d and AOD of the same kind of aerosol are almost linearly related to the emissions (or the amount of precursors) on a global scale (Chin et al. 2001). Therefore, errors in emission flux will have a direct effect on model-simulated M_d and AOD. The dust emission flux is highly dependent on the determination of the properties in the atmospheric surface boundary layer and the ground surface conditions for dust mobilization. The estimation of dust emission flux in the model is very sensitive to the threshold wind velocity for dust erosion, which is still affected by factors that are not the same for every desert. For example, the consistently

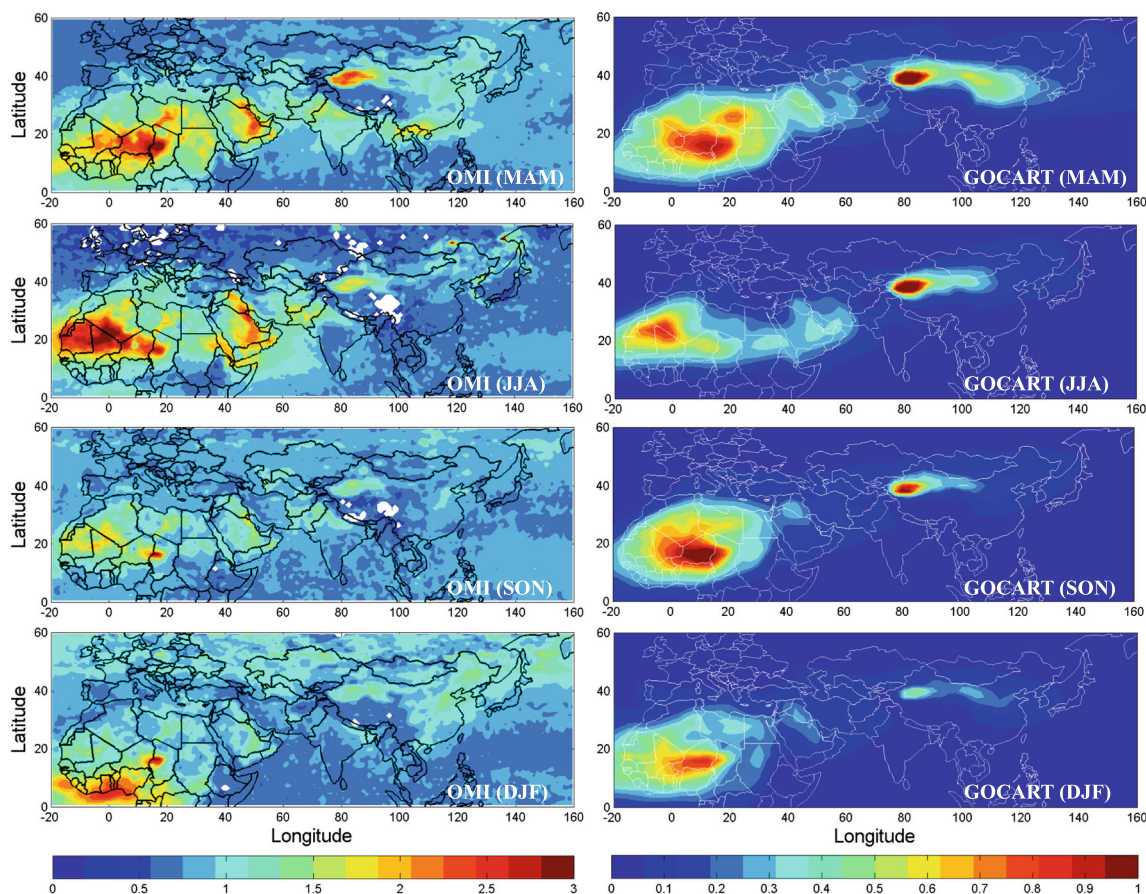


Fig. 3 Comparison between the seasonal distributions of the UVAI from OMI observations and dust AOD (550 nm) from GOCART simulations in 2007

overestimated dust AOD by GOCART over the Taklamakan Desert is likely caused by an excessive dust emission flux, which is most probably related to the inaccurate determination of threshold wind velocity. This can be explained by the Taklamakan Desert being higher in altitude than other deserts because it is closer to the Tibetan Plateau, the highest plateau in the world. Therefore, the properties of the atmospheric surface boundary layer over the Taklamakan Desert are different from those of other deserts, and this difference should have an effect on the determination of the threshold wind velocity over the Taklamakan Desert. But this property of the Taklamakan Desert is not considered in the calculation of threshold wind velocity, which is still treated uniformly for all deserts in GOCART to ensure numerical simulation efficiency.

If aerosol dry mass is given, we can determine the quantity B according to the aerosol's microphysical and optical properties, which are actually not constant and vary depending on the atmospheric environment in which the aerosol is transported. For example, under some given meteorological conditions, dust particles can adsorb the moisture in the atmosphere by acting as condensation nuclei, or they can even combine with other kinds of aerosol particles, especially soluble aerosols like sulfate and nitrate. These physical and chemical transitions for dust particles obviously have direct and indirect effects on their microphysical and optical properties. However, the model cannot take into account all these transitions related to aerosol properties and can only highly parameterize the properties in order to improve computation efficiency.

The monthly mean profiles of dust extinction in the troposphere below 12 km from CALIPSO Lidar level 3 aerosol product data are used in this study. According to the UVAI distribution shown in Fig. 3, the cross sections passing over the major dust source regions have been selected to make sure the CALIPSO observed dust extinction in these cross sections that just present the characteristics of the dust plume emitted from the local source, not other sources. The location of these cross sections is shown in Fig. 1. Figure 4 compares the dust extinction in these cross sections from CALIPSO observation and GOCART simulation for individual desert source (550 nm).

As seen in the cross sections, GOCART simulations for every individual desert dust can capture the seasonal variation of vertical extension of dust plume in large scale: dust reaches the lowest altitude in winter and the highest altitude in spring or summer. The seasonal variation of vertical distributions of the low level contours (0.03–0.06) of dust extinction from CALIPSO observation can be simulated by GOCART, but the corresponding contour of Arabian, Karakum–Kavir, and Thar dust extinction from GOCART simulation is much

smaller in magnitude than the CALIPSO observation, and this is consistent with the results concluded from the comparison between GOCART simulated dust AOD and OMI observed UVAI (Fig. 3).

GOCART simulation can reproduce correctly the location of the dust source observed by CALIPSO, including the Sahara dust source between 10° and 20° E in winter, and the one between 0° and 20° E in autumn; Gobi dust source between 100° and 105° E, and between 115° and 120° E in winter; Arabian dust source around 25° N in summer and autumn; Karakum–Kavir dust source between 25° and 30° N, and between 25° and 30° N; and Thar dust source between 26° and 30° N. On the other hand, the dust emission calculation for these dust sources in GOCART simulation is inadequate because the value of dust extinction at the location of these dust sources simulated by GOCART is smaller than the CALIPSO observations.

The comparison between GOCART simulation and CALIPSO observation indicates that GOCART simulation for every individual desert dust source can reproduce the seasonal and large spatial scale characteristics of dust plume emitted from the simulated source but do not capture the pronounced feature in small spatial scale. This limitation is caused mainly by the coarse vertical resolution of GOCART model, which is 30 layers from the ground to 0.01 hPa, while the vertical resolution of CALIPSO data is 208 layers from the surface to 12 km altitude.

Dust transport to coastal East Asia

In order to reveal the season in which most dust particles can be transported to coastal East Asia, Fig. 5 shows the seasonal distributions of every desert dust AOD which are retrieved from the corresponding simulation for individual desert dust respectively. At the same time, the vertical variation of dust concentration during long-range transport is shown in three profiles. The zonal vertical profiles are at two latitudes 40° N, representing the eastward transport on the north side of the Tibetan Plateau, and 20° N, representing the eastward transport on the south side of the Tibetan Plateau (Fig. 5, bottom row). The meridional vertical profile at longitude 115° E can further show the dust concentration distribution after arriving in East Asia (Fig. 6).

Associated with the winter monsoon in East Asia (Lee et al. 2010), Gobi dust has a larger influence on coastal East Asia in spring and winter when more dust particles spread southward into coastal East Asia south of 30° N, resulting in the regional AOD being larger than 0.02. Because a lot of dust particles are uplifted into the

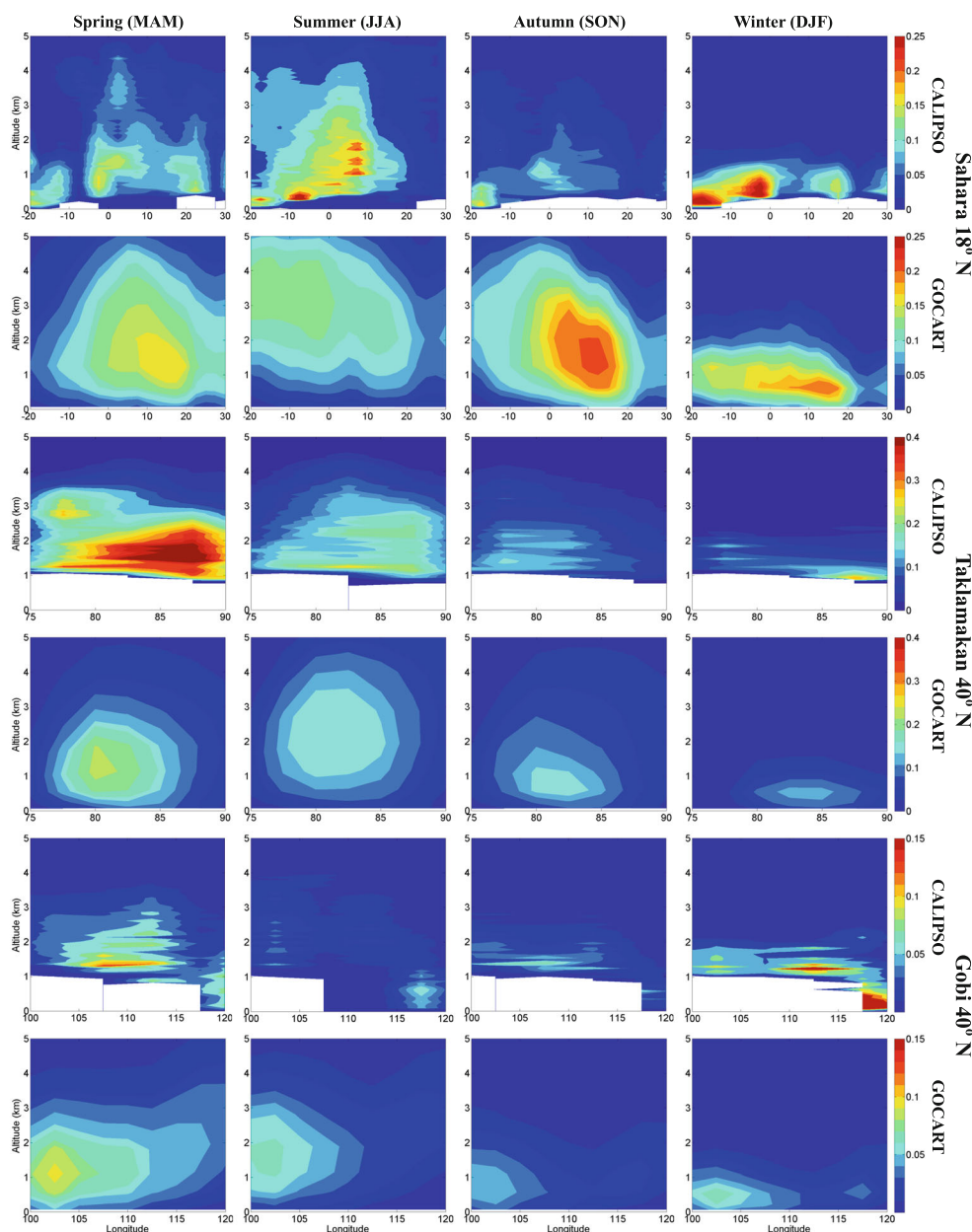


Fig. 4 Comparison of the vertical distribution of desert dust extinction in cross sections from GOCART simulations (550 nm) and CALIPSO observations (532 nm) in 2007

atmosphere by the frequent dust storms in spring, the spring Gobi dust AOD over coastal East Asia is larger than that in winter, with an increase from 0.02 to 0.2. In spring, the Gobi dust concentration over coastal East Asia (around 120° E) is about $100 \mu\text{g m}^{-3}$, extending vertically from the surface to an altitude of 700 hPa (Fig. 5, zonal vertical profile at 40° N). Shown by the meridional vertical profile at 115° E in spring, the maximum dust concentration appears above the surface around 40° N, being larger than $150 \mu\text{g m}^{-3}$, while the corresponding dust concentration at lower latitudes from 20° to 30° N is in the range of $10\text{--}100 \mu\text{g m}^{-3}$.

In spring, a Sahara dust band with an AOD above 0.05 expands eastward a long distance across the Middle East, Central Asia, and northeastern Asia to arrive at the North Pacific Ocean, while it becomes weaker in winter. The location of this band certainly agrees with the transport pathway of Sahara dust to East Asia demonstrated by Lee et al. (2011), which includes a track from the eastern Mediterranean region to the Middle East subtropical jet, the polar jet, and the East Asian subtropical jet (Lee et al. 2011). In addition, the eastward transport of Sahara dust is divided into two branches by the Tibetan Plateau, and the branch on the south side of the Tibetan Plateau just passes across the Indian subcontinent. In

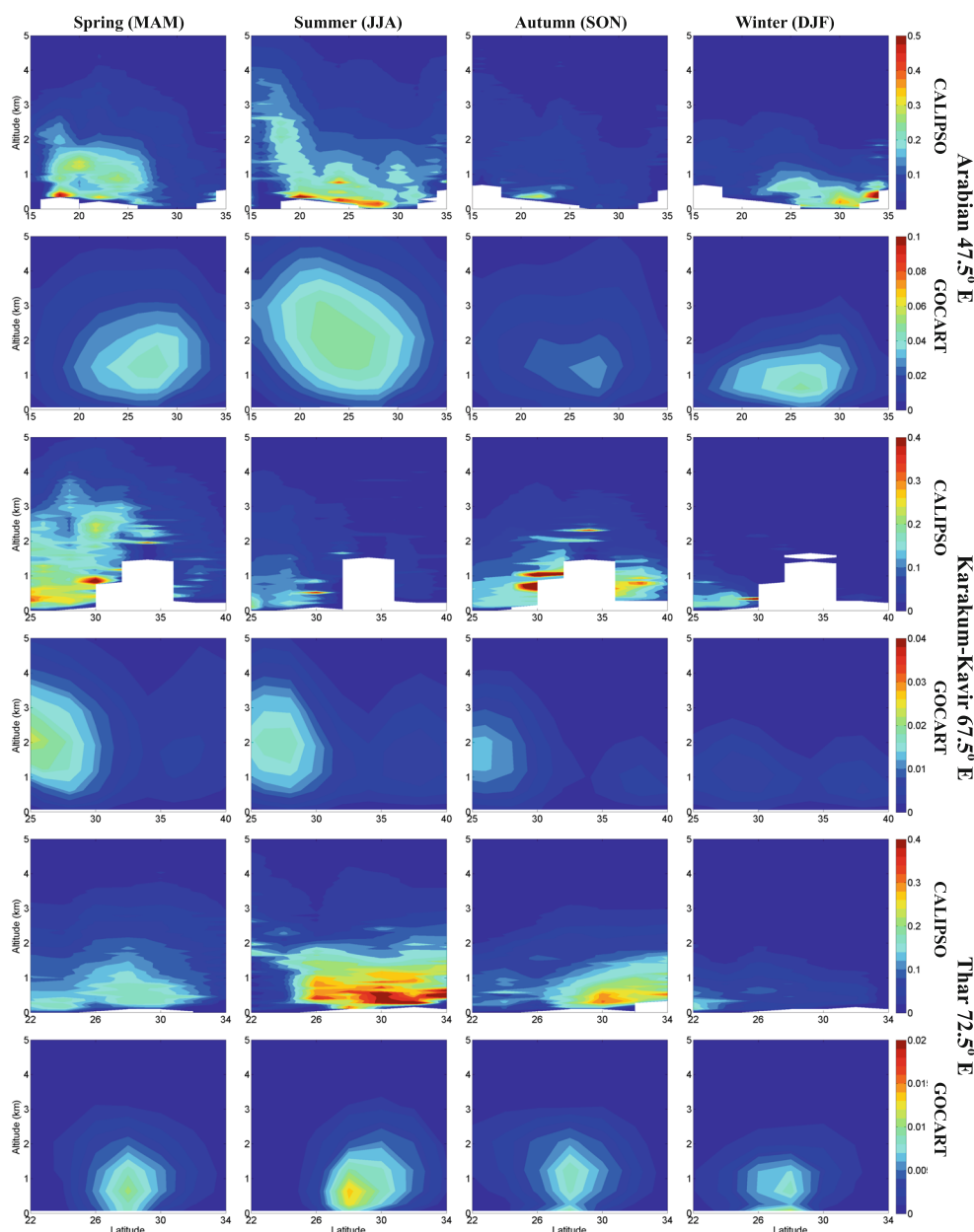


Fig. 4 continued.

spring, the contribution of Sahara dust to the AOD over coastal East Asia south of 30° N is larger than 0.02 (Fig. 5). The Sahara dust arriving in coastal East Asia (around 120° E) appears mainly in the middle troposphere (700–400 hPa), with the concentration being larger than $10 \mu\text{g m}^{-3}$ (zonal vertical profile at 40° N in Fig. 5). The dust plume, shown in the meridional vertical profile at 115° E in spring, exists mainly in the upper atmosphere at 700 hPa. The maximum concentration, appearing at 35° N, is larger than $18 \mu\text{g m}^{-3}$, while the dust concentration at lower latitudes (20° – 30° N) varies from 4 to $16 \mu\text{g m}^{-3}$.

Huang et al. (2007) analyzed CALIPSO data and found that in summer, the impact of Taklamakan dust on the

downwind Tibetan Plateau is larger than that derived from previous surface observations. In our study, the dust emitted from the Taklamakan Desert has a higher impact on coastal East Asia in summer than it does in other seasons, especially south of 25° N, where the AOD is larger than 0.02. The Taklamakan dust over coastal East Asia (around 120° E) dominates the middle to upper troposphere (700–200 hPa), where the dust concentration is larger than $10 \mu\text{g m}^{-3}$ (Fig. 5, zonal vertical profile at 40° N). The center of the dust plume at lower latitudes (20° – 30° N) occurs at an altitude of 400 hPa (Fig. 6). Although the Taklamakan Desert is close to the Gobi Desert, it differs in that Gobi dust transport is impacted by the Asian monsoon, while Taklamakan dust transport is impacted

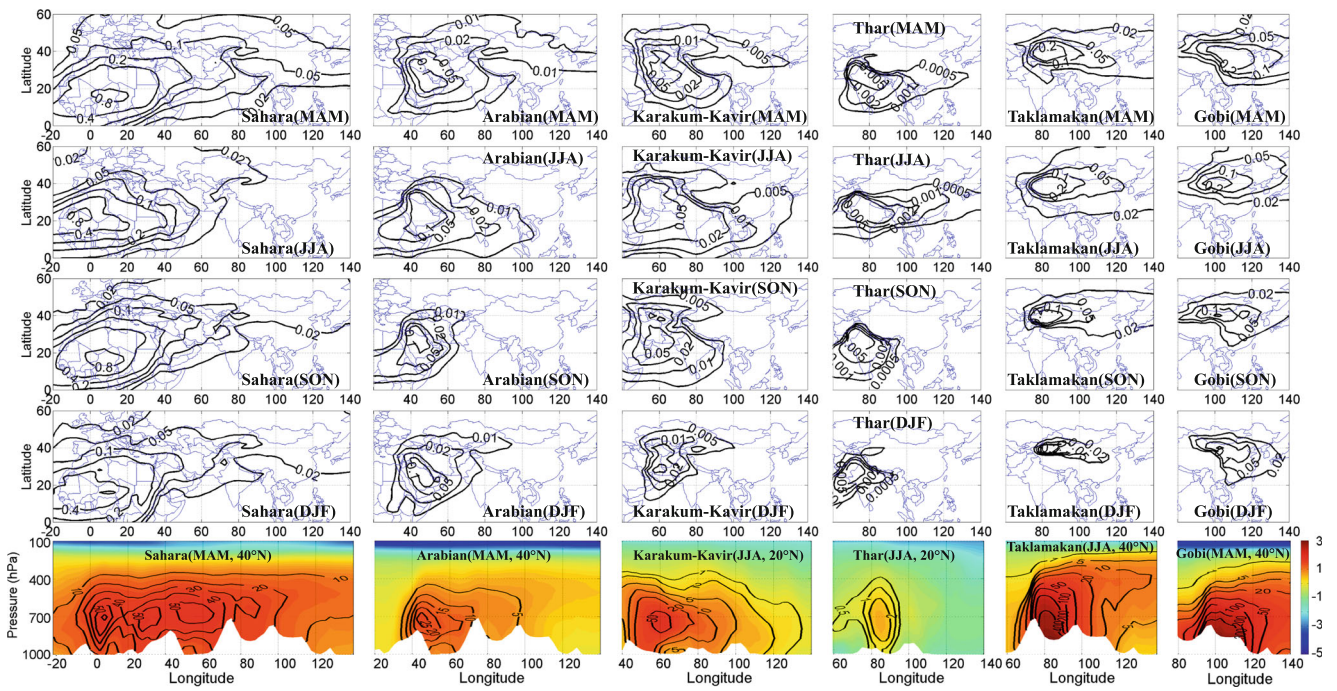


Fig. 5 Each desert dust AOD (550 nm) distribution (top 4 rows) and concentration (unit: $\mu\text{g m}^{-3}$) in zonal vertical profile at 20° or 40° N (on logarithmic scale; *bottom row*). The value of the *solid line* is the AOD or concentration value

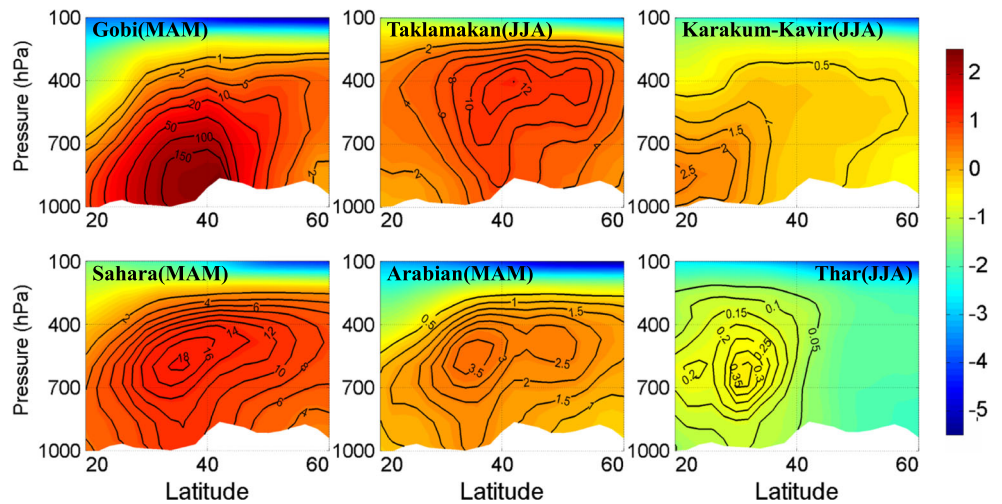
mainly by its specific topography. West China, where Taklamakan Desert is located, is so high in altitude that the East Asian monsoon cannot cover it; therefore, the transport of Taklamakan dust to coastal East Asia occurs in the upper atmospheric layer that cannot be controlled by the monsoon.

Arabian and Karakum–Kavir dusts have the same transport pattern to coastal East Asia: they transport eastward via the north side of the Tibetan Plateau in spring and via the south side of the Tibetan Plateau in summer. But the spring transport is more obvious for Arabian dust, while the summer transport is more apparent for Karakum–Kavir dust. The Arabian dust

concentrations shown by the zonal vertical profile at 40° N in spring, and the Karakum–Kavir dust concentrations shown by the zonal vertical profile at 20° N in summer, are more than $1 \mu\text{g m}^{-3}$ in coastal East Asia (120° E). The meridional vertical profile at 115° E further shows that the Arabian dust plume in spring occurs mainly in the middle troposphere (600–500 hPa) north of 30° N, and the Karakum–Kavir dust plume in summer occurs mainly in the lower troposphere (900–800 hPa) south of 30° N.

Via the south side of the Tibetan Plateau, Thar dust is transported eastward in a narrow band to coastal East Asia

Fig. 6 Dust concentration (unit: $\mu\text{g m}^{-3}$) in the meridional vertical profile at 115° E (on logarithmic scale). The value of the *solid line* is the concentration value



around 30° N in summer; therefore, this transport is not apparent in the zonal vertical profile at 20° N. But in the meridional vertical profile at 115° E, the Thar dust plume occurs mainly in the middle troposphere (800–500 hPa) in summer, and the maximum appear at 30° N at 700 hPa.

Variability and composition of urban dust concentration in coastal East Asia

In this section, we select two cities in coastal East Asia, namely Shanghai and Hong Kong, to study the variability and composition of their dust concentration. Shanghai and Hong Kong play an important role in East Asia because they are the top financial centre in the world. On the other hand, the population density of these two cities is larger than that of other cities in East Asia. Therefore, the quality of environment of these two cities, especially the air quality, can have potential huge effect on human health and activities, even on the economic development of East Asia. Hong Kong is located in South China, centered at 114.25° E and 22.25° N, at the mouth of the Pearl River where it meets the South China Sea. Shanghai is located in East China, centered at 121.48° E and 31.18° N, at the mouth of the Yangtze River where it meets the East China Sea.

It is noted that because the resolution of the GOCART model is 2.5° longitude by 2° latitude, larger than the real size of Shanghai and Hong Kong, the GOCART-simulated results for Shanghai and Hong Kong are actually the spatial average of the grid cell that includes Shanghai and Hong Kong. If the aerosol is emitted from local source in one grid cell, its concentration should show obvious spatial variation in this grid cell. Therefore, the aerosol concentration in a city located in this grid cell cannot be represented by the spatial mean value of aerosol concentration in this grid cell. But now, we are studying the impact of long-range transport of dust, even the intercontinental transport. Dust particles have mixed very well in the atmosphere after the long-range transport process. Therefore, in the downstream grid cell which includes Hong Kong and Shanghai, the spatial variation of dust concentration is very small. The dust concentration in the city located in this grid cell should very close to the spatial mean value of dust concentration in this grid cell. Another notice is that, for the grid cell which includes Hong Kong and Shanghai, its area except for the city is covered mainly with water, without dust source. Therefore, for the dust concentration in this grid cell, there is no contamination from local source.

Temporal and vertical variations in dust concentration are illustrated in Fig. 7 in Shanghai and Hong Kong, and it can be seen that most dust particles are concentrated in

the troposphere. The wet deposition of dust is related with the cloud and precipitation which is formed mainly in the middle troposphere layer. Therefore, the troposphere is further divided into the following three sublayers: the upper (500–200 hPa), middle (800–500 hPa), and lower troposphere (ground surface–800 hPa). Correspondingly, Fig. 8 further shows the monthly variation of the composition of dust concentration in the upper, middle, and lower troposphere.

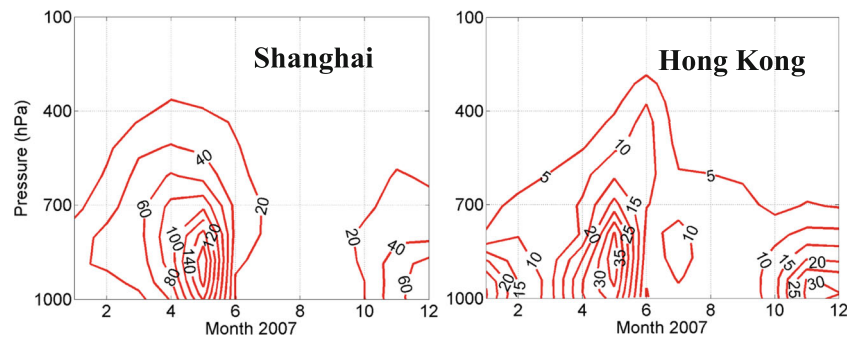
The dust concentrations in Shanghai and Hong Kong show many similar features in seasonal variation and composition. The seasonal variation of dust concentration exhibits two maxima: one in the winter caused by the dust in the lower troposphere (Shanghai, more than 60 $\mu\text{g m}^{-3}$ in December; Hong Kong, 29 $\mu\text{g m}^{-3}$ in November), and the other in the spring (May), controlled mainly by the dust in the middle (Shanghai, 85 $\mu\text{g m}^{-3}$; Hong Kong, 21 $\mu\text{g m}^{-3}$) and lower troposphere (Shanghai, 163 $\mu\text{g m}^{-3}$; Hong Kong, 37 $\mu\text{g m}^{-3}$). For these maxima, Gobi dust is generally the first major component, followed by Sahara and Taklamakan dusts, while their percentage contributions show vertical variation in the subtropospheric layer.

For dust concentrations in spring (March–May), the Gobi dust ratio shows a vertically upward decrease, i.e., for the peak dust concentration in May; the contribution of Gobi dust in the lower troposphere (88 % in Shanghai; 58 % in Hong Kong) is larger than that in the middle troposphere (67 % in Shanghai; 26 % in Hong Kong) because of Gobi dust transport to coastal East Asia in the lower troposphere (see the “Dust transport to coastal East Asia” section). On the other hand, the contribution of Sahara dust displays a vertically upward increase for dust concentration in spring, because its transport to coastal East Asia exists mainly in the middle and upper troposphere (see the “Dust transport to coastal East Asia” section). For the same reason, the contribution of Taklamakan dust displays a vertically upward increase for dust concentration in summer (June–August).

Also of note is that in spring, affected by the southward diffusion, the concentrations of Gobi, Sahara, and Taklamakan dust in Hong Kong (lower latitude) are smaller than that in Shanghai (higher latitude), but the relatively sharp decrease of Gobi dust concentration during its southward dispersion makes the Sahara and Taklamakan dusts in Hong Kong account for a greater percentage than in Shanghai, compared with the Gobi dust accounting for a smaller percentage in Hong Kong than in Shanghai.

Karakum–Kavir dust makes its largest contribution in the lower troposphere during summer (Shanghai, 22 % in July; Hong Kong, 41 % in August), corresponding to its transport to coastal East Asia in the lower troposphere in summer. In addition, the percentage of Karakum–Kavir dust in Hong Kong is larger than that in Shanghai, because it enters East Asia via the south side of the Tibetan Plateau.

Fig. 7 Temporal and vertical distributions of the dust concentration (unit: $\mu\text{g m}^{-3}$) in Shanghai and Hong Kong in 2007



Arabian dust has two strong impacts on Shanghai and Hong Kong: one in spring (March) and the other in summer (July). The impact in spring (March) can be seen from the high concentration of Arabian dust in the middle troposphere in Shanghai ($4.6 \mu\text{g m}^{-3}$) and Hong Kong ($1.6 \mu\text{g m}^{-3}$). At this time, the transport of Arabian dust to coastal East Asia via the north side of the Tibetan Plateau makes its concentration in Shanghai larger than that in Hong Kong. However, the contribution of Arabian dust in Shanghai (10 %) is smaller than that in Hong Kong (27 %), which results from the comparatively large concentrations of Gobi, Sahara, and Taklamakan dust in Shanghai. The impact of Arabian dust in summer (July) is represented by the percentage contribution in the

lower troposphere in Shanghai (24 %) and Hong Kong (31 %). In addition, the percentage value in Hong Kong is larger than that in Shanghai, corresponding to the transport of Arabian dust to coastal East Asia via the south side of the Tibetan Plateau in summer (see the “Dust transport to coastal East Asia” section).

Variability and composition of urban wet deposition of dust in coastal East Asia

The variations of the convective and large-scale wet deposition of dust in Shanghai and Hong Kong in 2007, and the corresponding percentage contribution of their

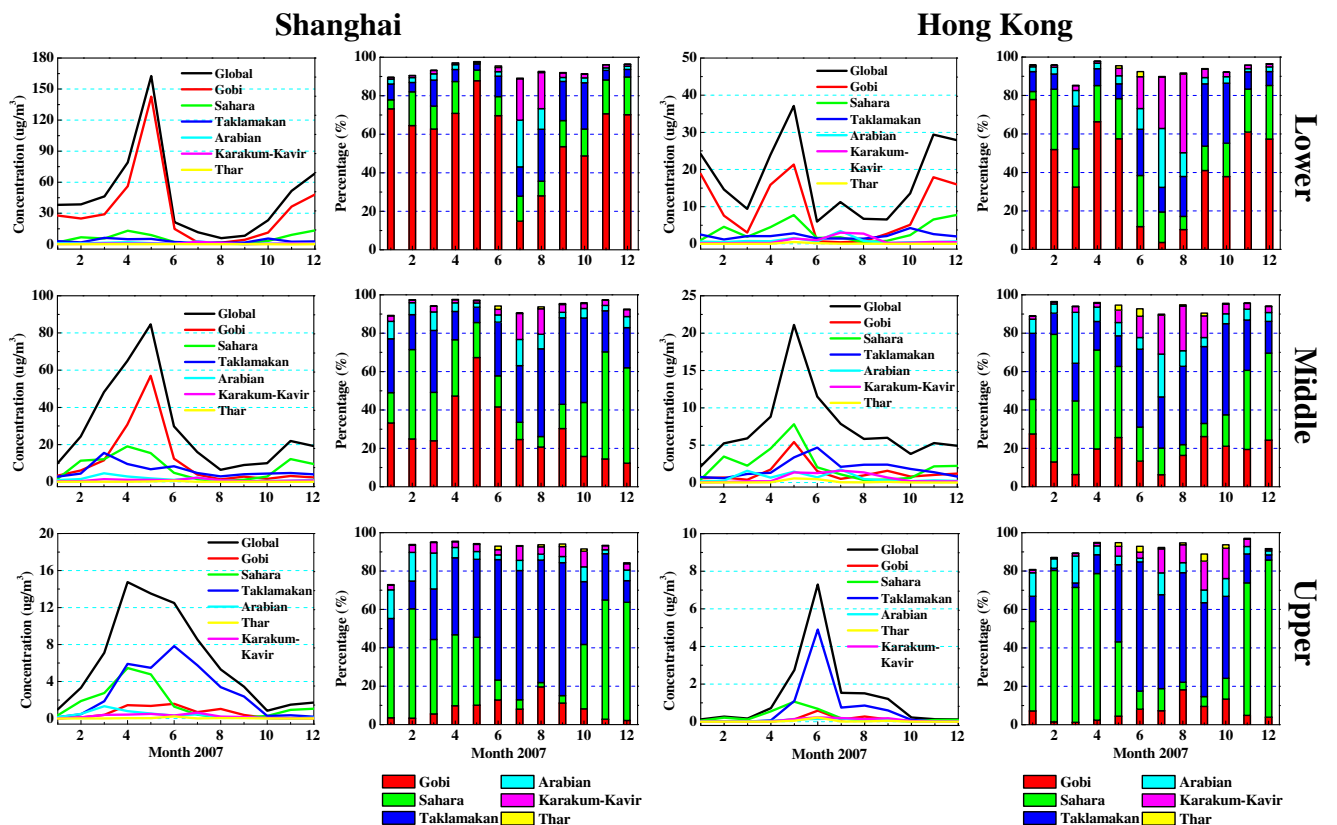


Fig. 8 Temporal variation of dust concentration and composition contribution in the troposphere sublayers in Shanghai and Hong Kong in 2007

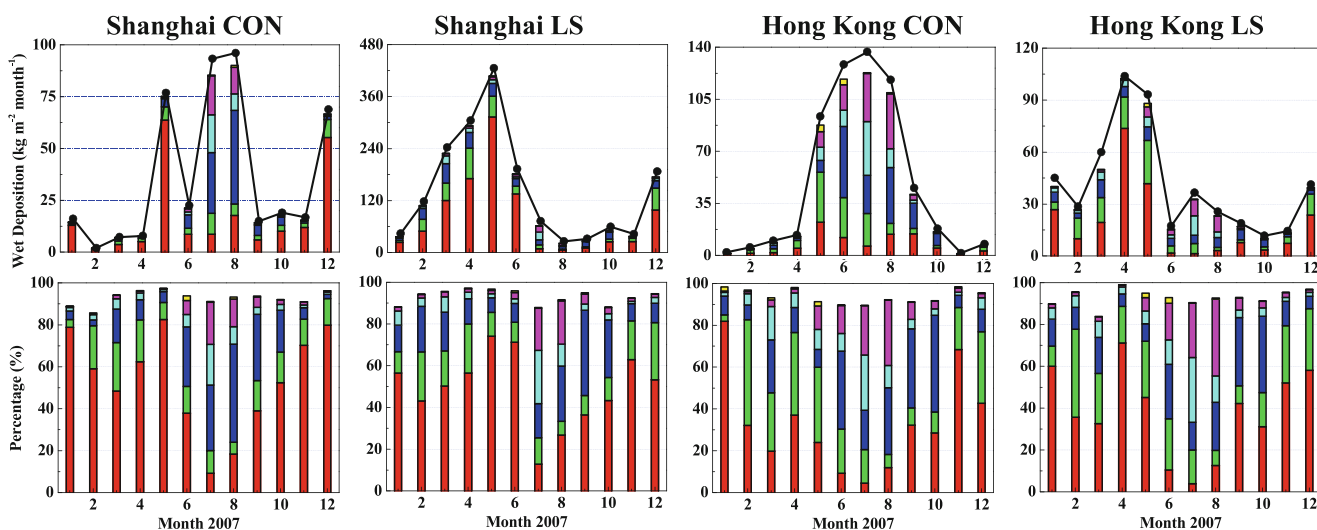
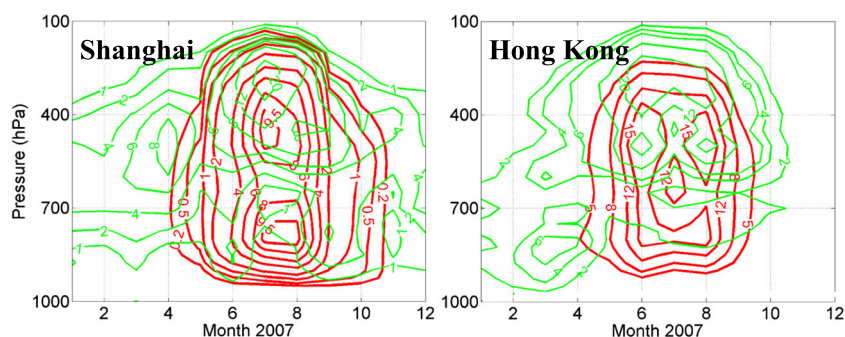


Fig. 9 Temporal variation of convective (CON) and large-scale (LS) wet deposition of dust in Shanghai and Hong Kong in 2007 (*top row*) and the composition contribution (*bottom row*); colored bars are the same as in Fig. 8. Solid circle is the wet deposition from global sources

composition, are presented in Fig. 9. Because the wet deposition of dust is related with the precipitation, we select the precipitation production rate as the reference parameter to discuss how the precipitation in Shanghai and Hong Kong affect the wet deposition of dust. The precipitation production rate data are retrieved from the dataset of the Modern Era-Retrospective Analysis for Research and Applications (MERRA). As reanalysis, MERRA dataset makes extensive use of satellite observations (Rienecker et al. 2011). Therefore, it is very close to the real phenomenon and is fit to be used in this study. The precipitation production rates in Shanghai and Hong Kong in 2007 are shown in Fig. 10. The data are gridded into the same resolution as the GOCART model to make an accurate analysis.

Because the wet deposition of dust occurs when dust particles are scavenged out by rainfall, the variation in wet deposition depends on the following two factors: (1) dust concentration and (2) the amount of precipitation, including both convective and large-scale precipitation. Here, we divide the wet deposition of dust in Shanghai and Hong Kong into three groups: one is caused mainly by high dust concentration, and the others come from strong convective and large-scale precipitation.

Fig. 10 Temporal and vertical distributions of the precipitation production rate (unit: $\mu\text{g kg}^{-1} \text{s}^{-1}$) in Shanghai and Hong Kong in 2007; red contour lines are the convective precipitation, and green contour lines are the large-scale and anvil precipitation, with those in summer generally being anvil precipitation



Wet deposition mainly from convective precipitation

Wet deposition in summer is affected mainly by convective precipitation, while the dust concentration at this time is very small. In summer, the convective wet deposition of dust in Hong Kong ($117\text{--}139 \text{ kg m}^{-2} \text{ month}^{-1}$ in June–August) is larger than that in Shanghai ($93\text{--}96 \text{ kg m}^{-2} \text{ month}^{-1}$ in July–August) because the convective precipitation in Hong Kong is stronger than that in Shanghai (Fig. 10).

Demonstrated by the vertical distribution of the precipitation production rate from convection in summer, convective precipitation develops in the whole troposphere, with the core existing in the middle troposphere. Therefore, the dust particles that form convective wet deposition in summer come mainly from the middle troposphere. Correspondingly, the percentage contribution of convective wet deposition is mostly similar to the contribution of the concentration in the middle troposphere. Taklamakan dust in West China dominates the wet deposition in summer (31–47 % in Shanghai; 19–37 % in Hong Kong), followed by Arabian dust in the Middle East and Karakum–Kavir dust in Central Asia. The percentages of Arabian and Karakum–Kavir dust in Hong Kong (Arabian

8–27 %; Karakum–Kavir 13–31 %) are larger than those in Shanghai (Arabian 8–19 %; Karakum–Kavir 13–20 %) because they enter East Asia via the south side of the Tibetan Plateau in summer.

Wet deposition mainly from large-scale precipitation

Wet deposition caused mainly by large-scale precipitation generally occurs in spring (April). The large-scale wet deposition of dust in Shanghai ($301 \text{ kg m}^{-2} \text{ month}^{-1}$) is twice as large as that in Hong Kong ($104 \text{ kg m}^{-2} \text{ month}^{-1}$). For composition, Gobi dust from Mongolia dominates large-scale wet deposition, followed by Sahara dust from North Africa and Taklamakan dust from West China.

In Hong Kong, because large-scale precipitation in April occurs in the lower troposphere (seen from the distribution of large-scale clouds, not shown here), the ratio of every desert dust in the wet deposition is very close to the ratio in the concentration in the lower troposphere, i.e., Gobi dust accounts for 71 % of the wet deposition and 66 % of the lower troposphere concentration. On the other hand, in Shanghai, the contribution of Gobi dust to the wet deposition (57 %) is apparently smaller than that in the lower troposphere concentration (71 %) but larger than that in the middle troposphere concentration (47 %).

Wet deposition from high dust concentration

In Shanghai, the peaks of convective and large-scale wet deposition in May seem to be determined mainly by the high dust concentration, compared with the weak precipitation at this time. For the composition, this kind of wet deposition is therefore dominated by Gobi dust (74–83 %), because Gobi dust is the majority of the high dust concentration, as discussed in the “Variability and Composition of Urban Dust Concentration in Coastal East Asia” section.

Summary and conclusions

The atmospheric chemical transport model GOCART is used in this study to quantitatively estimate the contributions of dust from different desert sources to the total dust concentration and wet deposition in the coastal cities of East Asia: Shanghai and Hong Kong. The temporal variation and spatial distribution of these contributions are further analyzed to determine their dependence on dust transport and other impacting factors.

The variation of every desert dust concentration and their contributions to the total dust concentration in Shanghai and Hong Kong are determined mainly by four factors: (1) the amount of source emissions, (2) the distance from the desert source to the city of deposition, (3)

the altitude of the desert source, and (4) the transport pathway of dust to East Asia. The dust concentrations in both Shanghai and Hong Kong exhibit maxima in winter and spring (May), and the majority of these maxima comes from the Gobi Desert because the distance from the Gobi Desert to the cities is shorter than that from other deserts. In addition, the concentration and contribution of Gobi dust in Shanghai are larger than that in Hong Kong, because Shanghai is closer to the Gobi Desert than Hong Kong. On the other hand, the contribution of Thar dust from the Indian subcontinent is smaller than that of other desert dusts because the Thar Desert has the smallest amount of emissions among these deserts. The Sahara Desert in North Africa is the farthest away from the cities, but the amount of its emissions is huge, larger than that of other desert sources, so Sahara dust is the second largest contribution. The Taklamakan Desert is so high in altitude that the transport of its dust to coastal East Asia during summer occurs in the upper atmosphere; correspondingly, Taklamakan dust makes the largest contribution to the dust concentration in the upper troposphere over Shanghai and Hong Kong during summer. The transport of Arabian dust from the Middle East to coastal East Asia via the north side of the Tibetan Plateau in spring makes its concentration larger at higher latitudes (Shanghai), but this transport changes to the south side of the Tibetan Plateau in summer, which makes the Arabian dust contribution larger at lower latitudes (Hong Kong). The transport pathway of Karakum–Kavir dust from Central Asia to East Asia via the south side of the Tibetan Plateau in summer leads to its larger contribution at lower latitudes (Hong Kong).

The variation in wet deposition of dust depends on two factors: (1) dust concentration and (2) the amount of precipitation, including both convective and large-scale precipitation. Wet deposition in summer is affected mainly by strong convective precipitation, while the dust concentration at this time is very small. With the core of the convective precipitation existing in the middle troposphere, the convective wet deposition has a similar composition to the dust concentration in the middle troposphere, being dominated by Taklamakan dust from West China (31–47 % in Shanghai; 19–37 % in Hong Kong), followed by Arabian dust from the Middle East and Karakum–Kavir dust from Central Asia. Wet deposition in spring (April) is caused mainly by large-scale precipitation, and the majority is Gobi dust from Mongolia (57 % in Shanghai; 71 % in Hong Kong), followed by Sahara dust from North Africa and Taklamakan dust from West China. In Shanghai, the peaks of wet deposition occur in May, including convective and large-scale deposition, and seem to be related with the high dust concentration, compared with the weak convective and large-scale precipitation at

this time, and this kind of wet deposition is apparently controlled by Gobi dust (74–83 %).

The variation in total wet deposition of dust (the sum of convective and large-scale wet deposition) has different patterns in Shanghai and Hong Kong. The total wet deposition in Shanghai shows similar seasonal variation to the dust concentration, with peaks in May and December, demonstrating that the wet deposition in Shanghai is affected mainly by the dust concentration. On the other hand, in Hong Kong, the total wet deposition becomes higher in May and July, demonstrating that the wet deposition in Hong Kong is controlled by both dust concentration and convective precipitation.

Acknowledgments This research is supported by the Natural Science Foundation at the Inner Mongolia University of Technology X201310 and National Science Foundation of China Grant 11362012.

References

- Allen DJ, Kasibhatla P, Thompson AM, Rood RB, Doddridge BG, Pickering KE, Hudson RD, Lin SJ (1996) Transport-induced inter-annual variability of carbon monoxide determined using a chemistry and transport model. *J Geophys Res* 101(D22):28655–28669
- Chin M, Diehl T, Ginoux P, Malm W (2007) Intercontinental transport of pollution and dust aerosols: implications for regional air quality. *Atmos Chem Phys* 7(21):5501–5517
- Chin, M, Ginoux, P, Holben, B, Chou, M-D, Kinne, S, Weaver, C (2001) The GOCART model study of aerosol composition and radiative forcing. http://acdb-ext.gsfc.nasa.gov/People/Chin/papers/Chin_ams_2001.pdf
- Chin M, Ginoux P, Kinne S, Torres O, Holben BN, Duncan BN, Martin RV, Logan JA, Higurashi A, Nakajima T (2002) Tropospheric aerosol optical thickness from the GOCART model and comparisons with satellite and sun photometer measurements. *J Atmos Sci* 59(3):461–483
- Chin M, Rood RB, Lin SJ, Müller JF, Thompson AM (2000) Atmospheric sulfur cycle simulated in the global model GOCART: model description and global properties. *J Geophys Res* 105(105):24671–24688
- Duce RA (1995) Sources, distributions, and fluxes of mineral aerosols and their relationship to climate. In: Charlson RJ, Heintzenberg J (eds) *Dalhem workshop on aerosol forcing of climate*. Wiley, New York, pp. 43–72
- Gillette DA, Passi R (1988) Modeling dust emission caused by wind erosion. *J Geophys Res* 93(D11):14233–14242
- Ginoux P, Chin M, Tegen I, Prospero JM, Holben B, Dubovik O, Lin SJ (2001) Sources and distributions of dust aerosols simulated with the GOCART model. *J Geophys Res* 106(D17):20255–20273
- Giorgi F, Chameides WL (1986) Rainout lifetimes of highly soluble aerosols and gases as inferred from simulations with a general circulation model. *J Geophys Res* 91(D13):14367–14376
- Huang J, Patrick M, Yi Y, Qiang T, Xin W, Hu Y, Liu Z, Ayers K, Trepte C, Winker D (2007) Summer dust aerosols detected from CALIPSO over the Tibetan Plateau. *Geophys Res Lett* 34(18):529–538
- Jickells TD, An ZS, Andersen KK, Baker AR, Bergametti G, Brooks N, Cao JJ, Boyd PW, Duce RA, Hunter KA, Kawahata H, Kubilay N, laRoche J, Liss PS, Mahowald N, Prospero JM, Ridgwell AJ, Tegen I, Torres R (2005) Global iron connections between desert dust, ocean biogeochemistry, and climate. *Science* 308(5718):67–71
- Kim HS, Chung YS, Yoon MB (2016) An analysis on the impact of large-scale transports of dust pollution on air quality in East Asia as observed in central Korea in 2014. *Air Qual Atmos Health* 9(1):83–93
- Koepke, P, Hess, M, Schult, I, Shettle, EP (1997) Global aerosol data set. Max-Planck-Inst, Meteorology Hamburg report no. 243, 44 pp.
- Lee YC, Wenig M, Larko D, Zhang Z, Diehl T (2011) Dust episodes in Hong Kong (South China) and their relationship with the Sharav and Mongolian cyclones and jetstreams. *Air Qual Atmos Health* 5(4):413–424. doi:10.1007/s11869-011-0134-7
- Lee YC, Yang X, Wenig M (2010) Transport of dusts from East Asian and non-East Asian sources to Hong Kong during dust storm related events 1996–2007. *Atmos Environ* 44(30):3728–3738
- Mahowald NM, Baker AR, Bergametti G, Brooks N, Duce RA, Jickells TD, Kubilay N, Prospero JM, Tegen I (2005) Atmospheric global dust cycle and iron inputs to the ocean. *Glob Biogeochem Cycles* 19(4):1064–1067
- Mctainsh G, Strong C (2007) The role of aeolian dust in ecosystems. *Geomorphology* 89(s1–2):39–54
- Nishikawa M, Kanamori S, Kanamori N, Mizoguchi T (1991) Kosa aerosol as eolian carrier of anthropogenic material. *Sci Total Environ* 107(91):13–27
- Okin GS, Mahowald N, Chadwick OA, Artaxo P (2004) Impact of desert dust on the biogeochemistry of phosphorus in terrestrial ecosystems. *Glob Biogeochem Cycles* 18(2):649–655
- Prospero JM (1996) The atmospheric transport of particles to the ocean. In: Ittekkot V, Schaffer P, Honjo S, Depetris PJ (eds) *Particle flux in the ocean*. Wiley, New York, pp. 19–52
- Rienecker MM, Suarez MJ, Gelaro R, Todling R, Bacmeister J, Liu E, Bosilovich MG, Schubert SD, Takacs L, Kim GK, Bloom S, Chen J, Collins D, Conaty A, da Silva A, Gu W, Joiner J, Koster RD, Lucchesi R, Molod A, Owens T, Pawson S, Pegion P, Redder CR, Reichle R, Robertson FR, Ruddick AG, Sienkiewicz M, Woollen J (2011) MERRA–NASA’s modern-era retrospective analysis for research and applications. *J Clim* 24(14):3624–3648
- Shao Y, Wyrwoll KH, Chappell A, Huang J, Lin Z, Mctainsh GH, Mikami M, Tanaka TY, Wang X, Yoon S (2011) Dust cycle: an emerging core theme in Earth system science. *Aeolian Res* 2(4):181–204
- Tegen I (2003) Modeling the mineral dust aerosol cycle in the climate system. *Quat Sci Rev* 22(18–19):1821–1834
- Torres O, Tanskanen A, Veihelmann B, Ahn C, Braak R, Bhartia PK, Veefkind P, Levelt P (2007) Aerosols and surface UV products from ozone monitoring instrument observations: an overview. *J Geophys Res* 112:177–180. doi:10.1029/2007JD008809
- Zhang Z, Wenig M, Zhou W, Diehl T, Chan KL, Wang L (2014) The contribution of different aerosol sources to the aerosol optical depth in Hong Kong. *Atmos Environ* 83(8):145–154